ACS APPLIED MATERIALS & INTERFACES

RESEARCH ARTICLE

www.acsami.org

Lyotropic Liquid Crystalline Self-Assembly Material Behavior and Nanoparticulate Dispersions of a Phytanyl Pro-Drug Analogue of Capecitabine—A Chemotherapy Agent

Xiaojuan Gong,[†,⊥] Minoo J. Moghaddam,[†] Sharon M. Sagnella,[†] Charlotte E. Conn,[‡] Stephen J. Danon,[†] Lynne J. Waddington,[§] and Calum J. Drummond*[,‡]

[†]CSIRO Materials Science and Engineering, PO Box 184, North Ryde, NSW 1670, Australia

[‡]CSIRO Materials Science and Engineering, Bag 10, Clayton South, VIC 3169, Australia

[§]CSIRO Materials Science and Engineering, 343 Royal Parade, Parkville VIC 3052, Australia

[⊥]University of Sydney, School of Chemistry, NSW 2006, Australia

Supporting Information

ABSTRACT: An amphiphile prodrug, 5′-deoxy-5-fluoro-N^4-(phytanyloxycarbonyl) cytidine (5-FCPhy) has been prepared and investigated for its self-assembly material properties, in vitro cytotoxicity, and in vivo efficacy as a chemotherapy agent. The phase transitions and stability of the neat amphiphile were characterized by differential scanning calorimetry (DSC) and thermogravimetric analysis (TGA). X-ray diffraction (XRD) was used to confirm the structure of the neat amphiphile, which was an amorphous glassy material. The lyotropic liquid crystalline self-assembly behavior of the amphiphile prodrug in water was examined by cross polarizing optical microscopy (POM) and small-angle X-ray scattering (SAXS). Under excess water conditions at room temperature, the amphiphile prodrug self-assembles into lyotropic liquid crystalline mesophases of inverse bicontinuous cubic symmetry. Upon aging, the inverse cubic phase slowly transformed to an inverse hexagonal phase. This amphiphile was successfully dispersed into nanoparticles of cubic and hexagonal symmetry. The in vitro cytotoxicity of dispersed nanoparticles was evaluated in seven different normal and cancer cell types and exhibited IC_{50} values between 70 and 90 μM for all cell types. Evaluation of 5-FCPhy in vivo against a mouse 4T1 breast tumor model displayed a trend of increasing efficacy with increasing dose. Furthermore, after 21 days, tumor volumes in the 0.5 mmol 5-FCPhy treatment group were significantly smaller than all other treatment groups including mice receiving a short chain water-soluble analogue, Capecitabine (a commercially available oral chemotherapy agent), delivered at the same dosage.

KEYWORDS: pro-drug, amphiphile, self-assembly, 5-fluorouracil (5-FU), cubosome, Capecitabine

INTRODUCTION

A prodrug is a chemically modified version of a toxic drug, with reduced systemic toxicity. The prodrug is activated at the specific site of action via an enzymatic or biochemical reaction.[1] Prodrug modification is often used to increase the lipophilicity of a drug thereby improving passive membrane permeation. One common method of creating a prodrug has been covalent attachment of a hydrophilic drug to a long alkyl chain that can then be hydrolyzed via an enzymatic reaction.[2,3] With this type of drug formulation, oral administration is possible because an increase in the drug lipophilicity can enhance drug uptake across the epithelial barrier of the gastrointestinal tract and thereby improve bioavailability. Thus, a prodrug strategy may overcome drawbacks associated with pharmacologically potent hydrophilic drugs, such as high toxicity and low bioavailability.

5-fluorouracil (5-FU) is a highly toxic chemotherapeutic drug that has played a dominant role in the treatment of breast cancer, colorectal cancer, and a variety of other solid tumors. Due to its hydrophilic nature, this drug has a very low absorption rate and low bioavailability. Capecitabine (Xeloda) has been developed to overcome some of the limitations of 5-FU.[4−9] Capecitabine is an inactive precursor of 5-FU, which is administered orally and, following rapid uptake, converts to the active form by a three-step enzymatic reaction in the liver and at the tumor site. It is currently the only oral 5-FU prodrug authorized by the U.S. Food and Drug Administration (FDA). Xeloda has been shown to possess a number of advantages over 5-FU including lower toxicity, improved bioavailability via oral administration, and tumor selective activation.[6,10,11] This prodrug is currently used to treat colon, metastatic colorectal and metastatic breast cancer. Following oral administration of Capecitabine, the 5-FU concentration in tumors has been shown to be several orders of magnitude higher than those treated with 5-FU either by oral or intravenous administration. Despite all of these advantages, this prodrug has a relatively high clearance rate and must be administered at relatively high doses twice per day.

The design of effective, sustained release delivery systems to circumvent the problem of high drug clearance rates is an ongoing challenge. One strategy is the use of nanoparticle-based delivery systems, consisting of either biodegradable polymers or lipid-based nanoassemblies, such as liposomes, for encapsulation

Received: January 27, 2011
Accepted: March 30, 2011
Published: March 30, 2011

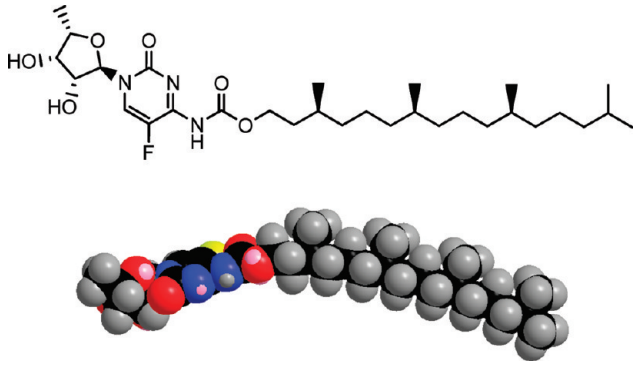

Figure 1. Chemical structure and energy minimized (space filling model) of the amphiphile prodrug 5-FCPhy.

of a wide range of toxic drugs.[1,12−17] Nanoparticles, either formed directly by drug conjugates or acting as carriers of chemotherapeutics, have been reported to promote passive targeting and drug penetration through the leaky neovasculature of tumors.[16,18,19] To date, liposomes represent the most widely studied lipid-based nanocarrier system and Doxil, a commercially available liposomal formulation of Doxorubicin, has been approved for the treatment of ovarian cancer.[18,20] Liposomes are dispersed nanoparticles of a liquid crystalline fluid lamellar phase. Amphiphilic molecules can also self-assemble into a variety of higher ordered nanostructures including 2D inverse hexagonal and 3D inverse cubic mesophases. These mesophases have been studied extensively in the last two decades for their high potential as drug delivery systems,[13,21] and as delivery agents in cosmetics and food.[22−24] The high surface area and extensive water channel networks in the higher-order liquid crystalline structures facilitate the incorporation of high payloads of both hydrophobic and hydrophilic drugs. More importantly, because of their size range, they have the potential to be targeted either passively or actively via incorporation of active targeting molecules.[13,25]

We, and others, have recently designed and characterized a large number of novel amphiphiles with the capacity to self-assemble into 2D and 3D lyotropic liquid crystalline phases, suitable for use as drug delivery systems.[26−32] Here, evolving structure−property relationships have been used to design a series of 5-FU amphiphile prodrug analogues of Capecitabine with the propensity to self-assemble into lyotropic liquid crystalline structure under physiological conditions.[33] In the work reported herein we build upon a previous communication[33] introducing amphiphile 5-FC prodrugs. Elsewhere we have also demonstrated that replacement of the short C5 pentyl chain within the Capecitabine molecule with a longer C16 alkyl chain (palmityl) altered the self-assembly behavior of the molecule.[34] Namely, substitution of the pentyl chain by palmityl in the water-soluble Capecitabine resulted in formation of a crystalline lamellar phase under excess water conditions. We have shown that this phase may be successfully dispersed into solid lipid nanoparticles (SLNs). Herein we attempt to promote liquid crystalline phase formation at room or physiological temperature by substitution of the pentyl group at the N^4 position with a hydrophobic isoprenoid-like branched C16 alkyl chain, forming 5-FC phytanyl, 5-FCPhy, Figure 1. We present herein the synthesis, physicochemical characterization of 5-FCPhy and the in vitro cytotoxicity and in vivo efficacy of its self-assembled amphiphile nanoparticles. Nanoassemblies of 5-FCPhy have been shown to undergo the first enzymatic conversion step, carboxylesterase hydrolysis to a 5-FC prodrug, at a much slower rate than Capecitabine (e.g., 26 h vs 15 min for full conversion under equivalent conditions).[33] The formation of liquid crystalline nanoparticles with a concomitant reduction in the enzymatic conversion rate, suggests potential for a sustained release of the drug, and thereby a lower clearance rate and more effective therapeutic properties.[33,34]

EXPERIMENTAL PROCEDURES

General Method. Materials preparation, characterization methods, and in vitro and in vivo experimental methods are similar to those described in refs 33 and 34 and are described briefly here. A full experimental method is therefore provided in the Supporting Information.

Thermogravimetric Analysis (TGA). The thermal decomposition weight loss was measured in the range 25 to 500 °C with a heating rate of 10 °C/min using a Mettler Toledo thermogravimetric analyzer TGA/SDTA 851^e (Mettler Toledo, Switzerland).

Differential Scanning Calorimetry (DSC). DSC curves were obtained using a Mettler Toledo (Mettler Toledo, Switzerland) differential scanning calorimeter DSC822^e equipped with a liquid nitrogen cooling system. All scans were heated at a fixed heating rate of 10, 2.5, or 0.2 °C/min. The enthalpy change associated with each thermal transition was obtained by integrating the area of the relevant DSC peak. The transition temperatures and energies were determined with the Mettler combined STAR SW8.10 software.

X-ray Diffraction (XRD). XRD analysis was performed on a PANalytical X′pert PRO X-ray diffractometer. A solid crystal sample was compressed into a thin film of 1 cm^2 area in the middle of a glass slide. Samples were analyzed at room temperature over a range of 2−80° 2θ with a step size of 0.05° 2θ, with each step measured for 60s.

Cross-Polarized Light Microscopy (Water Penetration Scans). An initial assessment of the lyotropic mesophase behavior was carried out using water penetration experiments. A small amount of neat amphiphile was placed on a glass slide, and covered with a glass coverslip. Drops of Milli-Q water, introduced to the edge of the coverslip, resulted in a concentration gradient from pure amphiphile in the center to pure water around the edges of the coverslip. The generated mesophases were identified by their characteristic textures using an Olympus GX51 inverted polarizing microscope (Olympus Australia Pty.Ltd., Australia) equipped with an Olympus C-5060 digital camera for image capture.

Small-Angle X-ray Scattering (SAXS). Excess water samples were analyzed using an Anton-Paar SAXSess (Graz, Austria) with a PANalytical PW3830 stand-alone X-ray generator operating at 40kv, 50 mA with a sealed-tube Cu anode ($\lambda_{Cu-K\alpha}$ = 0.154 nm). All measurements were performed in the heating direction with equilibration times of 10 min at each temperature.

All other samples were analyzed using the SAXS/WAXS beamline at the Australian Synchrotron. The experiments used a beam of wavelength λ = 0.80 Å (15.0 keV) with dimensions 700 μm × 500 μm and a typical flux of 1.2 × 10^{13} photons/s. 2D diffraction images were recorded on a Mar CX165 detector with analysis in the q-range 0.012−0.35 $Å^{-1}$.

Preparation of Colloidal Dispersions. The dispersions 5′-deoxy-5-fluoro-N4-(phytanyloxycarbonyl) cytidine (5-FCPhy) were prepared by a combination of sonication and extrusion. Neat prodrug containing 10% (wt/wt% lipid) of the triblock polymer stabilizer F127 was dissolved in a small amount of absolute ethanol and then added dropwise into milli-Q water with vigorous vortexing. The mixture was sonicated for two hours using a benchtop sonicator and then extruded through a series of polycarbonate (PC) membranes. The final concentration of the 5-FCPhy mixture was: 4.74% of 5-FCPhy, 0.45% F127, 9% ethanol, and 85.7% of water.

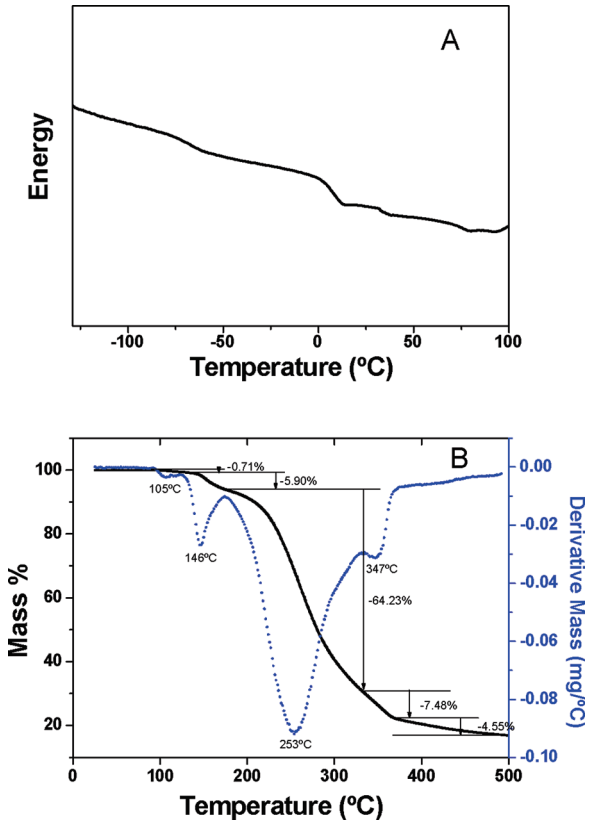

Figure 2. (A) DSC curve of 5FCPhy measured at 2.5 °C/min showing two glass transitions. (B) TGA trace (solid line) and 1st derivative curve (dotted line) of neat amphiphile prodrug 5-FCPhy.

Particle Size Distribution. Determination of the particle size distribution of the dispersions was carried out using dynamic light scattering (DLS) analysis on a Zetasizer (nano zs, Malvern) equipped with a He−Ne Laser (4mw, 633 nm) and an avalanche photodiode detector. The size distribution was recorded by intensity.

Cryo-Transmission Electron Microscopy (Cryo-TEM). Cryo-TEM Imaging was carried out using an FEI Tecnai 12 TEM, operating at 120 kV, equipped with a MegaView III CCD camera and Analysis imaging software (Olympus Soft Imaging Solutions). The sample was kept at a temperature of −180 °C and standard low-dose procedures were used to minimize radiation damage.

Molecular Modeling. The energy minimum conformation of the molecule was determined by Chem 3D Pro v11.0 (Cambridgesoft Corporation) using its MM2 energy minimization routine. The theoretical molecular distances of the hydrophobic and hydrophilic parts are determined from Sybyl 8.0 programs.

Cell Culture. The toxicity of the 5-FCPhy prodrug nanoparticles was evaluated against seven different cell types: MCF-7 (human breast cancer cell line; American Tissue Type Collection, USA), PC-3 (human prostate cancer cell line; kind gift from Prof. P. J. Russell, Institute of Oncology, Prince of Wales Hospital, UNSW, Australia), 4T1 (murine breast tumor cell line; kindly supplied by Dr F. Miller, Michigan Cancer Foundation, Detroit, MI, USA), HMEpiC (Primary human mammary epithelial cells; ScienCell, USA), PZ-HPV7 (human prostate epithelial cell line; kind gift from Prof. P. J. Russell, Institute of Oncology, Prince of Wales Hospital, UNSW, Australia), HH (human hepatocytes; ScienCell, USA), and MRC-5 (lung fibroblast cell line; ATCC, USA).

Antiproliferative Activity. Ten microliter aliquots of prodrug were added to the cells listed above with a final amphiphile prodrug concentration in five different logarithmic concentrations (100, 10, 1, 0.1, 0.01 μg/mL). The number of cells was determined by measuring the conversion of a tetrazolium compound into a formazan product by the mitochondria of living cells (CellTiter 96 AQ_{ueous} One Solution Cell Proliferation Assay, Promage, Australia). After ∼3 h incubation with the reagent, the absorbance was read at λ = 490 nm using a Wallac Victor 1420 multilable counter (Perkin-Elmer Life Science).

Table 1. DSC Scan Results Performed on Neat 5-FCPhy at Heating Rate 2.5 °C/min[a]

DSCscan rate (°C/min)	1st glass transition T_g onset (°C) [midpoint (°C)]	2nd glass transition T_g onset (°C) [midpoint (°C)]	visual melting point (°C)
2.5	−75.53 [−69.51]	3.80 [8.15]	53−68
	−66.31 [−66.38]	3.75 [7.20]	
	−73.36 [−68.95]	3.46 [7.56]	

[a] Thermal properties of three independent measurements of 5-FCPhy observed by DSC included two glass transitions, one near −70 °C, the other around 3 °C. Melting points obtained from visual observation are also listed. By visual observations, neat 5-FCPhy appeared as a sticky solid at temperatures below −20°C and became a clear sticky solid at ambient temperature.

In vivo Experiments. Female BALB/c mice were injected with 5×10^4 4T1 cells/10 μL PBS into the second mammary fat pad on the right-hand side. Mice were divided into 7 groups of 6 and administered the following daily treatments for 21 days calculated based on a 20 g mouse: 0.5 mmol of 5-FCPhy, 0.25 mmol o 5-FCPhy, 0.1 mmol of 5-FCPhy, 0.5 mmol of Capecitabine, 0.25 mmol of Capecitabine, 0.1 mmol of Capecitabine, or a 1.5 mg/mL solution of F127 in water. The length and breadth of the tumors were measured and recorded on day 1, 4, 7, 14, and 21 of drug administration. On day 22 of drug administration, mice were euthanized. Blood was collected via cardiac puncture, followed by removal of the tumor, liver, spleen, and kidney for histological analysis. Lungs were injected with indium ink prior to removal to allow for quantification of the number of lung metastases in each animal.

RESULTS AND DISCUSSION

Structural Studies on the Neat Amphiphile. *Differential Scanning Calorimetry (DSC).* At room temperature, neat 5-FCPhy appears as a sticky, highly viscous mesomeric wax. DSC of neat 5-FCPhy displayed two step-like transitions indicative of glass transitions (T_g) with onset temperatures at approximately −73 and 3.5 °C (Figure 2A). T_g values determined from DSC scans are presented in Table 1. No detectable melting peak was exhibited in the DSC trace at temperatures below the decomposition temperature of 5-FCPhy, however, visual observations on a sample heated from −20 °C on a hot stage showed a softening of the 5-FCPhy material at around 50 °C, which became a mobile isotropic liquid above 70 °C (Table 1).

In general, the introduction of branched hydrocarbon chains tends to lower the melting point and associated melting transition enthalpy, because of disruption of well-ordered packing of the molecules. Amphiphiles with isoprenoid-type phytanyl chains exhibit melting point transition temperatures significantly lower than their n-alkyl chain counterparts.[28,35−37]

One possible explanation for the two apparent glass transitions displayed by 5-FCPhy is that it may contain two amorphous domains; a disordered (glassy) hydrophobic chain and a disordered (glassy) headgroup region, and that the two domains undergo separate glass transitions. When supercooled below the first glass transition temperature T_{g1} (−73 °C), both the chain

and headgroup domains are in an amorphous glassy state where molecular motion is 'frozen'. Upon heating to a temperature range between the two T_gs (−73 to 3.5 °C), the hydrophobic layer can move freely in a liquid state but the headgroup layer is still locked in the frozen position. Further energy uptake at temperatures above T_{g2} (3.5 °C) enables the headgroups to escape from the "frozen" mode, releasing the whole molecule into a liquid state. Hence, the glass transitions in pure 5-FCPhy observed upon heating involve mobility changes of the structural units but not the structure itself. A similar trend was observed in a chelating amphiphile, phytanyl ethylene diamine tetra acetic acid (EDTA).[38]

Thermogravimetric Analysis (TGA). The change in weight of the sample as a function of temperature ranging from 25 to 500 °C and its first derivate curve are displayed in Figure 2B. Thermal degradation of 5-FCPhy exhibited multiple, partially overlapping processes accounting for 85.8% of the total weight loss. A minor weight loss (−0.71%) is represented as the first peak in the first derivative curve from 91 to 125 °C. Successive mass losses occurred from 125 to 371 °C in three decomposition steps, with mass losses of 5.9, 64.2, and 7.5%, respectively, accounting for more than 77% of the total loss. A much slower process occurs from 371 to 500 °C (−4.5%). Compared to the decomposition of 5-FCPalmityl (5-FCPal) (120 °C), the decomposition of 5-FCPhy (90 °C) begins at a much lower temperature.[34] It was also found that when exposed to sustained heating (i.e., incubation in a 50 °C oven for three weeks), 5-FCPhy undergoes decomposition as indicated by color changes and confirmed by UPLC measurement (data not shown). Thus, temperatures should remain below 90 °C during short-term processing of the 5-FCPhy prodrug, whereas temperatures below 25 °C are preferred for long-term storage of this material.

XRD and SAXS on Neat Amphiphile. Neat 5-FCPhy is a waxy, sticky solid below 50 °C. The X-ray powder diffraction pattern obtained for neat 5-FCPhy at 25 °C, Figure 3A, shows a single broad peak in the wide angle region between 10 and 20 nm^{-1}, suggesting molten hydrocarbon chains. SAXS images obtained on the same sample at 25, 37, 50, and 70 °C also show a broad peak at a q-value of approximately 1.61 nm^{-1}, indicative of a weakly ordered material, Figure 3B. The presence of a weakly ordered material is in agreement with DSC data indicating that the second T_g occurs at ∼3.5 °C. Similar XRD diffraction patterns have been observed by us for other amphiphile molecules containing phytanyl chains.[38]

Structural Studies on Hydrated Amphiphile. *Water Penetration Studies.* Representative water penetration scans carried out on 5-FCPhy are shown in Figure 4. Immediately following water exposure, at 23 °C, an isotropic band was observed at the water−surfactant interface, Figure 4A. The fast invasion rate of this isotropic band suggested that this did not represent an ordered lyotropic liquid crystalline phase but rather a rapid uptake of water by the sample. This was confirmed by SAXS experiments which, following overnight equilibration, showed a very broad peak indicative of an amorphous material. After three days equilibration at room temperature, another isotropic band slowly formed and expanded into the interior of the sample, Figure 4B. The high stiffness of this band suggests it is a cubic phase. Increasing the temperature to 37 °C facilitated the formation of this cubic isotropic band, Figure 4C. After further incubation of 1 day, a texture characteristic of a coexisting hexagonal phase was observed, Figure 4D. We suggest this represents an inverse hexagonal phase based on the low hydration capacity

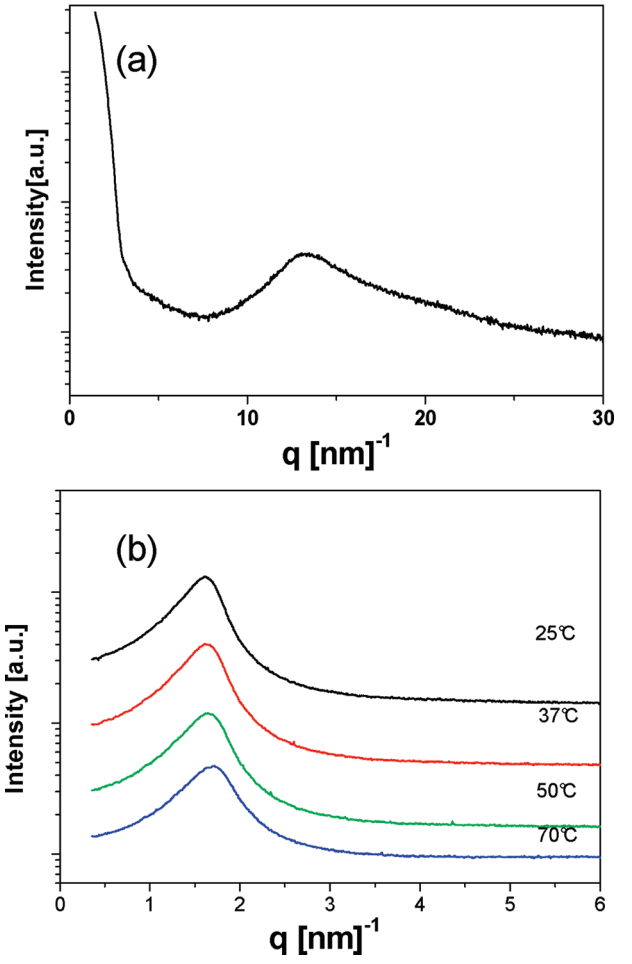

Figure 3. (A) XRD and (B) SAXS profile of neat 5-FCPhy.

of the mesophase and resistance to increased dilution. Both an increase in temperature and prolonged equilibration times favored the conversion of the cubic phase to an inverse hexagonal phase (H_{II}). The H_{II} phase progressively expanded into the neat surfactant phase, Figure 4E, F, and after 11 days of equilibration at 37 °C, the sample had completely converted to H_{II}. The rate of transition to the hexagonal phase can be accelerated to two days by maintaining the sample at 60 °C. This inverse hexagonal phase remained unchanged up to 90 °C. The mesophase structures of the isotropic band and the anisotropic band were confirmed to be a cubic Q_{II}^{D} phase of *Pn*3*m* symmetry and a hexagonal H_{II} phase, respectively, via SAXS experiments and are discussed further in the following section.

XRD and SAXS on Hydrated Samples. SAXS experiments were carried out across a range of water contents, in the temperature-range 25−70 °C. Typical 1D diffraction patterns are shown in Figure 5. The mesophase adopted and the associated lattice parameters calculated from the SAXS measurements are given in Table 2.

The weakly ordered material formed by neat 5-FCPhy at 25 °C is retained up to the temperature at which sample decomposition occurs. At a limited hydration of 9 wt % water SAXS data show a broad peak indicative of a fluid micellar phase, Figure 5A. Superimposed on the broad peak are two peaks at q-values of 1.820 and 1.904 nm^{-1} (25 °C) in the ratio $\sqrt{11}$: $\sqrt{12}$ marked with an asterisk. These peaks are retained as the water content is

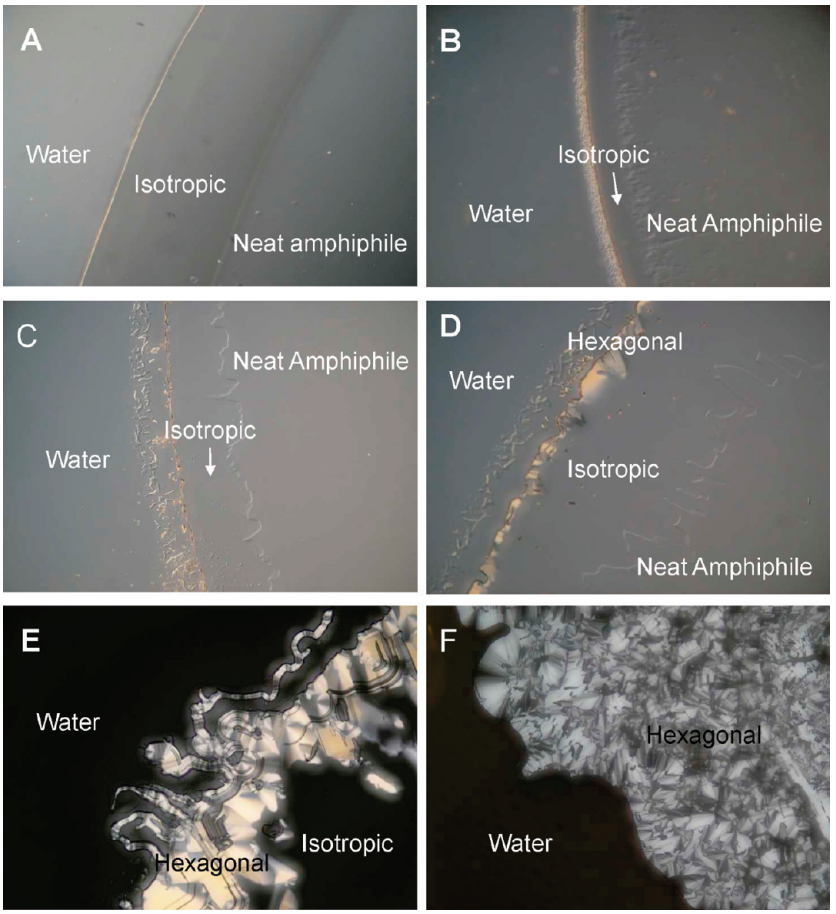

Figure 4. Water penetration scans of 5-FCPhy at varying temperatures and equilibration times. (A) 25 °C for 30 min. An isotropic band developed quickly at the interface of neat 5-FCPhy and water. (B) 25 °C for 6 days. A new isotropic band is observed at the water interface. (C) 37 °C for 4 days. An isotropic band is observed at the water interface. (D) 37 °C for 5 days. Four different regions exist, water, a birefringent region (H_{II}), an isotropic phase, and neat 5-FCPhy. (E) 37 °C for 11 days viewed through cross polarizers. The expansion of the H_{II} phase is observed. (F) 60 °C for 2 days viewed through cross polarizers. The whole sample has converted to H_{II} phase. 100× magnification.

increased, although they smear out into a single broad peak centered on a *d*-spacing of 32.9 Å by 30 wt % water. Peaks in this ratio may correspond to the third and fourth order reflections of an Fd3m phase. In this case no additional peaks corresponding to an Fd3m phase are noted, although a diffuse hump is observed for the 19 wt % water sample at a q-value of 1.555 nm^{-1} (25 °C), in the expected position of the $\sqrt{8}$ reflection, marked with an asterisk. In addition, the *Fd3m* phase is not generally observed for binary lipid−water systems, rather for ternary systems consisting of two lipids of different chain lengths, and water.[39] Finally, the intensity variation is not as expected for an Fd3m phase, where the $\sqrt{11}$ peak is expected to be the most intense. We therefore are unable to assign these peaks and suggest they represent a partially ordered phase.

At water contents between 19 wt % (Figure 5B) and 40 wt % (Figure not shown) the system adopts an inverse hexagonal H_{II} phase, in addition to the unidentified phase described above. The lattice parameter of the H_{II} phase decreases with increasing temperature as expected. In addition the lattice parameter increases with increasing hydration (Table 2).

For 5-FCPhy at 60 wt % water, a coexistence of Q_{II}^{D} and H_{II} phases was observed for equilibration times up to 39 days, Figure 5C. Six characteristic Bragg diffraction peaks in the ratio $2:\sqrt{3}:\sqrt{4}:\sqrt{6}:\sqrt{8}:\sqrt{9}$ are indexed as the 110, 111, 200, 211, 220, 211 reflections of a Q_{II}^{D} cubic phase (crystallographic space group Pn3m). The lattice parameter of the cubic phase remains constant upon further dilution (data not shown) indicating that the cubic phase is in equilibrium with excess water. An additional diffraction peak at a q value of approximately 1.2 nm^{-1} is assigned as the first diffraction peak of a putative H_{II} phase. As only one peak is observed, assignment is based on comparison with POM results as well as similarity in *d*-spacing to that observed for the pure H_{II} phase. Although a pure cubic phase was seen using cross-POM this was not detected in the SAXS measurements. At temperatures above 60 °C, a transition to a fluid isotropic L_2 phase is seen.

However with time, the system slowly transforms to produce a pure H_{II} phase. This process required up to two months at room temperature. However we found that raising the equilibration temperature to 60 °C for 2 days (premelting) with subsequent equilibration at 25 °C could also produce a pure H_{II} phase, Figure 5D. Three distinct Bragg diffraction peaks in the ratio $1:\sqrt{3}:\sqrt{4}$ are indexed as 100, 111, and 200 reflections of a 2D hexagonal lattice. The H_{II} phase is stable up to 70 °C and we note that the 5-FCPhy-water system showed no detectable chemical change via UPLC after two days equilibration at 60 °C. Note that the UPLC system used, with dual UV and ELSD detectors, is highly sensitive and can detect possible degradation of less than 0.1%. In

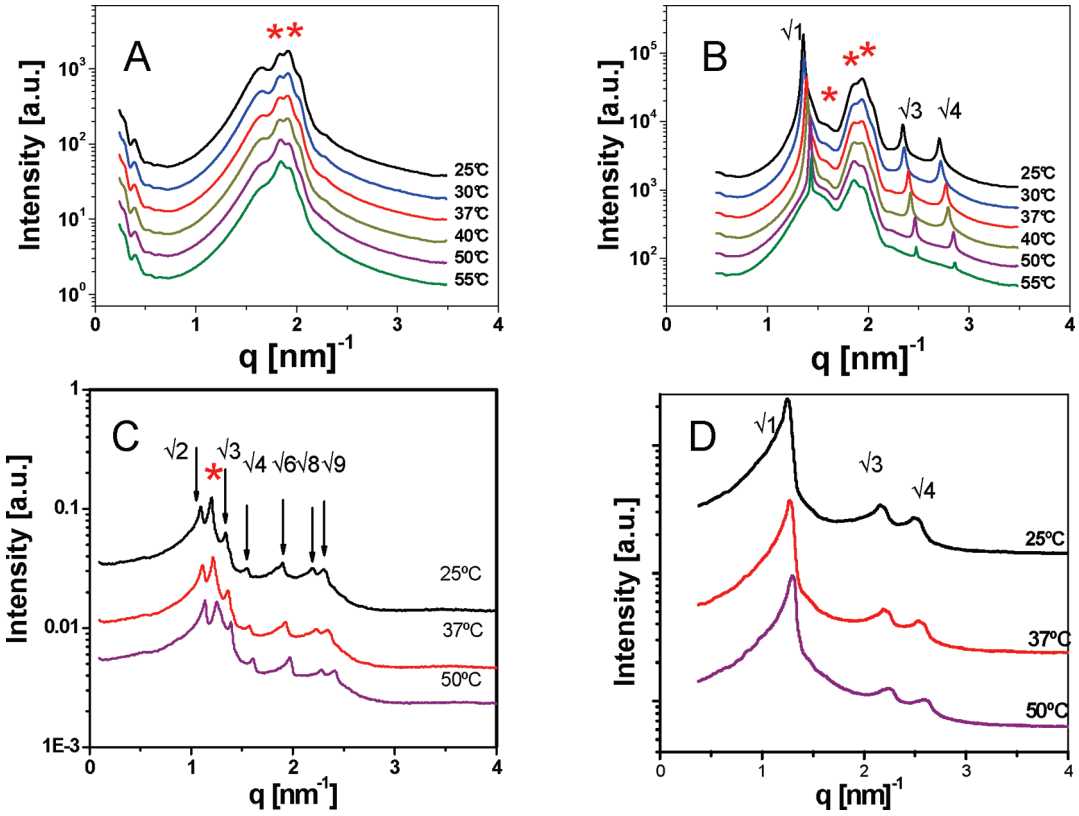

Figure 5. 1D SAXS diffraction patterns for samples at various water contents, temperatures, and equilibration conditions. (A) 5-FCPhy (9% water) without premelting, equilibrated at room temperature for 3 days. A diffuse peak corresponding to a L_2 phase is observed. Superimposed on this peak are unassigned peaks marked with an asterisk and discussed in the text. (B) 5-FCPhy (19% water) without premelting, equilibrated at room temperature for 3 days. The 1, $\sqrt{3}$, and $\sqrt{4}$ peaks of an inverse hexagonal H_{II} phase are observed. Additional unidentified peaks are marked with an asterisk and discussed in the text. (C) 5-FCPhy (60% water) without premelting equilibrated at room temperature for 3 days. The $\sqrt{2}$, $\sqrt{3}$, $\sqrt{4}$, $\sqrt{6}$, $\sqrt{8}$, and $\sqrt{9}$ peaks of a Q_{II}^D phase (*Pn3m* symmetry) are indicated. An additional peak, marked with an asterisk is assigned as the putative first-order reflection of a H_{II} phase. (D) 5-FCPhy (40% water) premelted and equilibrated at 60 °C for 2 days. The 1, $\sqrt{3}$, and $\sqrt{4}$ peaks of an inverse hexagonal H_{II} phase are indicated.

Table 2. Phase Behavior and Lattice Parameters of Neat and Hydrated 5-FCPhy Determined from XRD and SAXS Experiments; X, No Diffraction Observed

	water content (% w/w)						
	0	9	19	30	40	60	
temp (°C)			H_{II}	H_{II}	H_{II}	Q_{II}^D	H_{II}
25	weakly ordered	L_2	46.5	46.0	57.9	80.0	59.5
30	weakly ordered	L_2	46.3	45.6	57.5	79.4	58.5
37	weakly ordered	L_2	45.5	45.1	57.0	78.0	57.6
40	weakly ordered	L_2	45.1	44.6	55.7	77.4	57.1
50	weakly ordered	L_2	44.2	X	55.8	76.4	56.7
55	weakly ordered	L_2	X	X	55.6	X	X

Table 3. In vitro IC50 Values of Capecitabine,[7] 5-FCPhy, and 5FU Evaluated in Various Normal and Cancer Cell Lines; ND: Not Determined

	IC_{50} (μMI)		
cell culture	5-FCPhy	Capecitabine	5-FU
MCF7	94	>200	13[a]
HMEpiC	99	>200	ND
PC3	97	>200	7
PZHPV7	70	>200	ND
4T1	11	100	ND
MRC5	91	>200	ND
HH	99	100	ND

[a] This value was obtained from ref 7.

line with the POM results the phase conversion rate from coexisting cubic and hexagonal phase to a pure hexagonal phase is again found to depend strongly on the equilibration temperature. The formation of higher-order lyotropic liquid crystalline phases (such as those of hexagonal or cubic symmetry) has been shown to be a kinetically hindered process for several lipid systems.[40,41]

The lattice parameter of the Q_{II}^D and H_{II} phases decrease with increasing temperature, Tables 2 and 3. The reduction in lattice parameter on heating reflects the increased degree of disorder in the hydrocarbon chains with an increased interfacial curvature of the bilayer and a concomitant reduction in unit cell size. The surfactant−water penetration behavior of 5-FCPhy was similar to other isoprenoid-type surfactants with the formation of cubic phases and hexagonal phases at relatively low temperatures (at or below ambient temperature).[28,42]

Nanoparticle Dispersion Characterization. *Particle Size Distribution.* Kinetically stable colloidal particle dispersions were produced from 5-FCPhy using a combination of hydrotrope inclusion and extrusion. Because the neat prodrug 5-FCPhy is

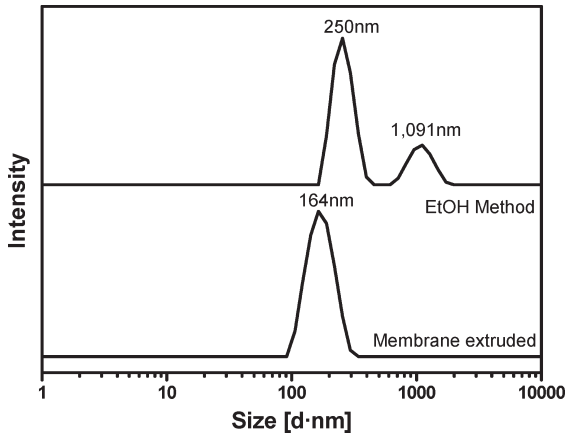

Figure 6. Particle size distribution (diameter in nm) as determined by dynamic light Scattering (DLS) of 5-FCPhy/F127/ethanol dispersions. Upper curve represents the coarse dispersions formed directly using the ethanol method. Bottom curve is the size distribution after size-controlled membrane extrusion.

sensitive to heating, no heating was used during the nanoparticle dispersion preparation. For 5-FCPhy which forms a coexistence of cubic Q_{II}^{D} and H_{II} phases in the presence of water, this method effectively produced a uniform dispersion. The dispersions are stabilized against aggregation by the addition of a nonionic triblock copolymer, Pluronic F127. The size distribution of the nanoparticle dispersion formed initially via hydrotrope inclusion and then followed by extrusion, is shown in Figure 6.

The 5-FCPhy dispersion appeared as an opaque, milky white solution. Prior to membrane extrusion, two particle populations were present ranging from 100 nm to few micrometers with two peaks located at 250 nm and ~1.1 μm respectively (Figure 6, upper curve). The volume fraction of particles larger than 800 nm occupied approximately 30% of the total volume of the particles. This coarse dispersion was directly passed through polycarbonate (PC) membranes for size reduction or subjected to weak sonication for a few hours to further break down the macroscopic particles and minimize the sample loss in the extrusion process. After consecutive membrane extrusion (30 cycles of extrusion per membrane of 1 μm, 800 nm, 400 nm, 200 nm and 100 nm membranes), only a single population remained with a mean particle size of 164 nm (Figure 6, lower curve). This demonstrates that extrusion treatment is an effective method for obtaining a uniform narrow size distribution for cubosomes and hexosomes, as well as liposomes.

The 5-FCPhy dispersions were stable for a few weeks at 25 °C in small aliquots. Stability was lower when stored in larger volume vials. The aggregate can easily be redispersed upon sonication or by passing through the extrusion membrane.

Cryo-TEM. Representative cryo-TEM images of 5-FCPhy colloidal nanoparticles under different conditions are shown in Figure 7. Similar to results obtained for bulk phase samples, the phase behavior of the dispersion was found to depend on the dispersion equilibration time and temperature. Samples equilibrated at room temperature for 2 weeks, Figure 7A and B, showed mostly cubosomes with very few hexosomes, as confirmed by fast Fourier transform (FFT) measurements. The majority of cubosomes possess a spherical shape rather than a square facet. This may be an artifact of the extrusion process; cubosomes with a spherical rather than a cubic shape have been previously observed for dispersions made by high shear techniques.[43] Direct structural evidence for the formation of cubosomes and hexosomes was obtained using high resolution cryo-TEM, Figure 7C, D. An individual cubosome structure is clearly seen in Figure 7C. When dispersions were equilibrated at 37 °C for 2 weeks, Figure 7D, structures characteristic of hexosomes were observed. Some particles exhibited the hexagonally faceted shape similar to that previously reported for a 2D projection of dispersed particles with hexagonal symmetry. Other particles had a characteristic multilamellar or fingerprint shape also indicative of hexosomes.[44−47] The particle size distribution observed from Cryo-TEM is in good agreement with DLS measurements.

SAXS on Nanoparticle Dispersions. As scattering from dispersed samples is weak, synchrotron SAXS was used to confirm the presence of order in the dispersed phase. Figure 8 shows the diffraction pattern obtained for a dispersion of 5-FCPhy in excess water following two weeks equilibration at 25 °C. Two distinct sets of well-defined diffraction peaks were seen corresponding to coexisting Q_{II}^{D} and Q_{II}^{G} phases. The Q_{II}^{D} phase was assigned as six peaks in the ratio $\sqrt{2}:\sqrt{3}:\sqrt{4}:\sqrt{6}:\sqrt{8}:\sqrt{9}$. Assignment of the Q_{II}^{G} phase was based on only two peaks in the ratio $\sqrt{6}:\sqrt{8}$. The lattice parameters of these phases were calculated as 78.5 Å for the Q_{II}^{D} phase and 124.4 Å for the Q_{II}^{G} phase. Although assignment of the Q_{II}^{G} phase is based on only two reflections the ratio of lattice parameters $a(Q_{II}^{G})/a(Q_{II}^{D}) = 1.585$ is close to that predicted for coexisting Q_{II}^{D} and Q_{II}^{G} phases (the Bonnet Ratio $a(Q_{II}^{G})/a(Q_{II}^{D}) = 1.576$).[48,49] The lattice parameter of the Q_{II}^{D} phase is slightly smaller than that obtained for the bulk cubic phase (80.3 Å) probably reflecting the addition of the polymer and ethanol required to disperse the bulk cubic phase.

The phase adopted by the dispersed nanoparticles differs from that of the bulk phase, where coexisting Q_{II}^{D} and H_{II} phases are observed, slowly transforming to a pure H_{II} phase with time. The formation of a coexisting Q_{II}^{G} phase for the dispersed samples is note-worthy as the Q_{II}^{G} phase is typically not observed under excess water conditions. However the behavior of dispersed nanoparticles has been shown in many cases to differ from the behavior of the bulk phase lipid. For example, Monoolein, which forms a Q_{II}^{D} (diamond) cubic phase in the bulk phase forms cubosomes of Q_{II}^{P} symmetry[50] and phytanyl monoethanolamide, which also forms a Q_{II}^{D} bulk phase, forms dispersed nanoparticles of cubic and hexagonal symmetry.[28] We suggest that the presence of the polymer used to disperse the system, along with the dispersion process has resulted in a change in phase. It has been documented that the self-assembly structure may be influenced by the addition of such external molecules.[44,51,52] In addition, the Q_{II}^{G} phase has been observed for cubosome systems that have not reached thermodynamic equilibrium,[53] again suggesting that phase transitions for the 5-FCPhy system may be kinetically hindered.

In vitro Toxicity. The 5-FCPhy nanoparticles and Capecitabine were examined for their toxicity against 7 different cell types consisting of both normal cells and cancer cell lines (Table 3). Capectabine is an effective chemotherapeutic agent which exhibits low toxicity in its parent form, thus limiting unwanted cytotoxic side effects. Because of the necessity of specific enzymes localized to the liver and tumor tissue in vivo for bioconversion of the prodrug to its active form, low toxicity in vitro is expected.

In vitro toxicity results demonstrate that 5-FCPhy exhibits slightly higher in vitro toxicity (IC_{50}) than Capecitabine for all

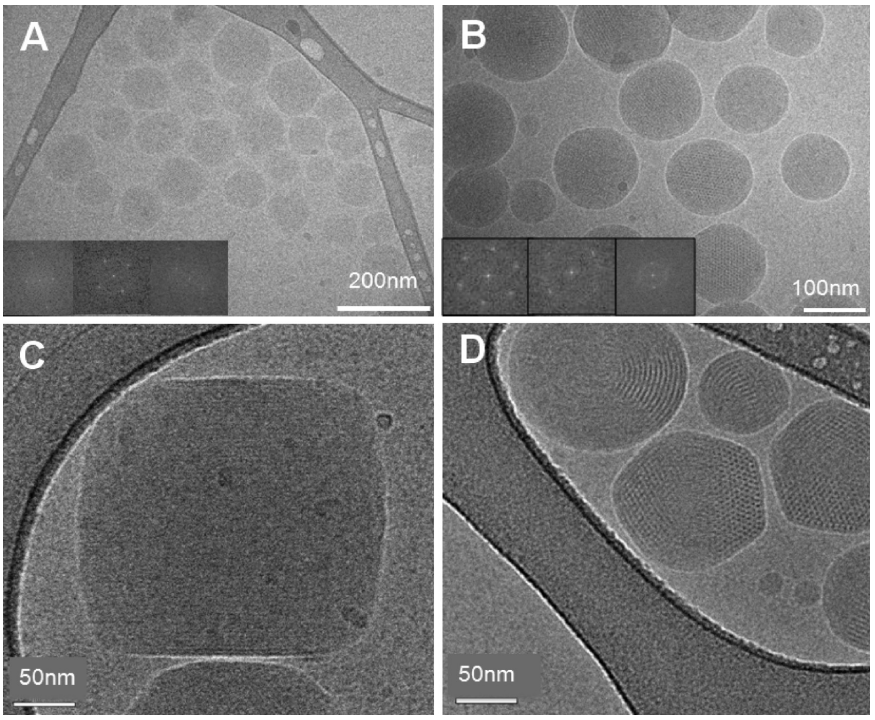

Figure 7. Cryo-TEM images and FFT (insets for A and B) of 5-FCPhy dispersions consisting of 4.74% 5-FCPhy, 0.45% F127, 9% ethanol, and 85.7% water. (A, B) Overview of a dispersion equilibrated at 25 °C for 2 weeks. The FFT of the internal structure of the particle shows both cubic and hexagonal arrangement. Typical examples of cubosomes (C) and hexosomes (D) obtained using a high-resolution FEI Tecnai 300F microscope equipped with a Gatan Ultrascan 1000UHS CCD camera.

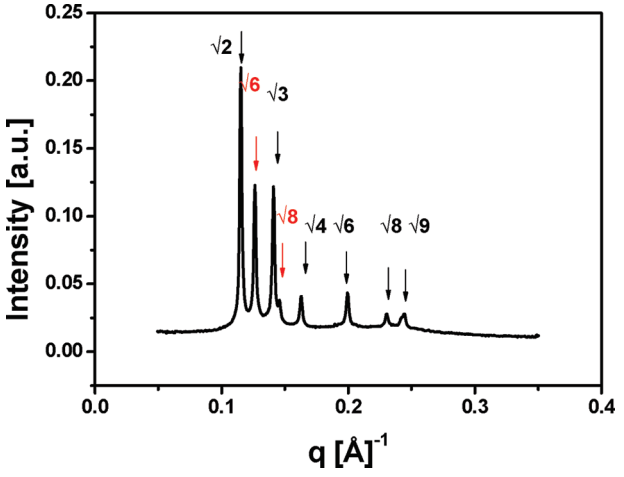

Figure 8. 1D Synchrotron SAXS diffraction pattern of a 5-FCPhy dispersion containing 4.74% 5-FCPhy, 0.45% F127, 9% ethanol, and 85.7% water. The $\sqrt{2}$, $\sqrt{3}$, $\sqrt{4}$, $\sqrt{6}$, $\sqrt{8}$, and $\sqrt{9}$ reflections of a Q_{II}^{D} cubic phase with *Pn3m* symmetry are seen. Two additional reflections in the ratio $\sqrt{6}$:$\sqrt{8}$ are indexed as a Q_{II}^{G} cubic phase of *Ia3d* symmetry.

cell types/lines examined. With the exception of the 4T1 cells (IC_{50}:11 μM), IC_{50} values for 5-FCPhy were between 70 and 90 μM for all cell types/lines. In contrast, IC_{50} values for Capecitabine were greater than 200 μM (the highest concentration examined) for all cell types/lines except the 4T1 and HH, which both had IC_{50} values of 100 μM. A two-step in vivo enzymatic activation process is needed to convert both 5-FCPhy and Capecitabine to 5-FU. 5-FU exhibits an IC_{50} of 13 μM to the MCF-7 cell line, which is 10-fold greater than 5-FCPhy. Reported IC_{50} values for 5-FU range from 0.25 μM to 22 μM in a variety of other human cancer cell lines.[7] Thus, low toxicity of 5-FCPhy is expected in vitro. Because of the unique bioactivation processes necessary to convert 5-FCPhy to its toxic form, it is unlikely that any toxicity exhibited in vitro can be attributed to the release of 5-FU from the prodrug form. Because of the formulation of 5-FCPhy into the highly fluid nanostructured nanoparticles, the in vitro toxicity can most likely be attributed to the nature of the interaction between the amphiphilic particles and the cell membrane. When a lipid containing nanoparticle interacts with the lipid bilayer of a cell membrane, fusion and lipid exchange can occur. If enough exchange occurs, disruption to the cell membrane integrity can occur and cell death may result. In the case of the 5-FCPhy nanoparticles, the hydrophobic portion of the molecule contains a highly branched phytanyl chain. The fluid nature of the nanoparticles could promote membrane fusion and amphiphilic exchange, while the branched nature of the hydrophobe may contribute to membrane instability. If enough particles interact with a particular cell, membrane integrity may fail and result in cell death. Because of the confined two-dimensional, static nature of the in vitro environment, the chances of this scenario occurring is much greater thus contributing to the lower IC_{50} values seen for the 5-FCPhy nanoparticles versus Capecitabine in vitro. However, we caution that these results are unlikely to be indicative of what may occur in the dynamic in vivo environment.

In vivo Efficacy. The efficacy of 5-FCPhy nanoparticles to the mouse 4T1 breast cancer model was assessed over a 21 day period at three different dosages (0.1 mmol, 0.25 mmol, and 0.5 mmol/mouse/day). For comparison, Capecitabine was administered at the

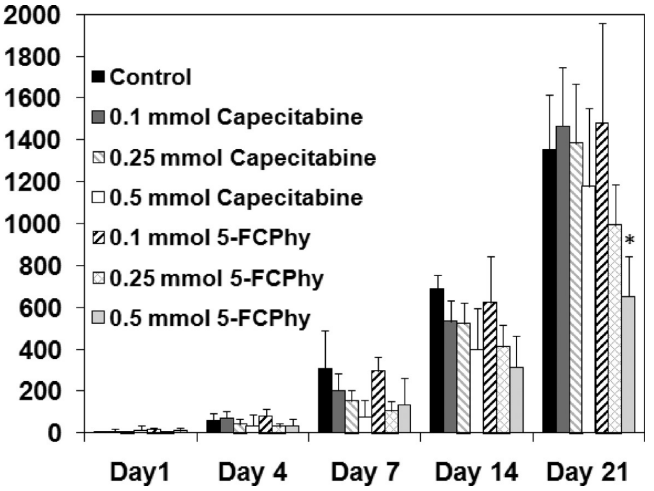

Figure 9. Average tumor size over a 21 day period for mice receiving either Capecitabine or 5-FCPhy nanoparticles at three different concentrations. Both drugs demonstrate improved efficacy in a dose dependent manner, with the intermediate and high dosages of 5-FCPhy exhibiting the smallest average tumor volumes at day 21. * 0.5 mmol 5-FCPhy significantly smaller than all other treatment groups.

same dosages to complementary groups of mice. A control group of mice received only a solution containing the F127 polymer stabilizer vehicle used in the particle formulation. Tumor volume was calculated by the following formula: volume = (breadth × length^2)/2. This formula is commonly used to calculate tumor volume for in vivo studies.[54] Average tumor sizes for all treatment groups are shown in Figure 9. On day 1 and day 4, tumors are relatively small in size, and no trend in treatment efficacy is visible. However, on day 7, a definite trend is visible in terms of decreasing average tumor size with increasing dosages of both the Capecitabine and 5-FCPhy treatment groups. Average tumor sizes for animals receiving the 0.1 mmol dose of both the 5-FCPhy and Capecitabine was comparable to the control mice receiving only the vehicle, indicating that this dosage was not sufficient to elicit a chemotherapeutic effect. In contrast, on day 21, animals receiving 0.25 mmol of 5-FCPhy had an average tumor size approximately 72% of those receiving both the control 0.25 mmol of Capecitabine and 84% of those receiving 0.5 mmol of Capecitabine. Furthermore, animals receiving the 0.5 mmol dose of 5-FCPhy had an average tumor size, which was less than 50% of the average tumor size in the control groups and 55% of the tumor size in the 0.5 mmol Capecitabine group on day 21. The average numbers of metastases seen in the lungs of the mice in the different treatment groups are shown in Table 4. Because of high variability, results are not statistically significant; however, both the 0.5 mmol dose of Capecitabine and 5-FCPhy had the lowest number of metastases, and numbers of metastases decreased in a dose-dependent manner.

The 0.5 mmol dose of 5-FCPhy display the highest efficacy of all treatments examined in terms of both average tumor volume and average numbers of lung metastases, however significance was only reached in terms of an average tumor volume on day 21 for the 0.5 mmol 5-FCPhy treatment groups compared to the control group. Small sampling size and the high variability which is inherent with in vivo studies resulted in no other statistically significant results. The formulation of 5-FCPhy in nanoparticulate form provides some advantages over Capecitabine. Enzymatic conversion of 5-FCPhy to its active form occurs at a significantly slower rate than Capecitabine, on the order of 26 h as compared to <15 min under equivalent environmental conditions.[33] The slower conversion of 5-FCPhy may allow for a more sustained delivery of 5-FCPhy than Capecitabine, and may not need to be delivered as often as Capecitabine. Here, we have administered 5-FCPhy following a daily dosing regime; however, because of the role of the internal nanostructure of the 5-FCPhy particles on its enzymatic conversion, similar efficacy is likely to be achieved via a less often dosing scheme. 5-FCPhy can also be tolerated at higher dosages, and thus we may be able to improve efficacy further by increasing the dosage. Additional in vivo studies are necessary to properly establish the sustained release capability and optimal dosage level of 5-FCPhy.

Table 4. Average number of lung metastases in each treatment group

treatment	average no. of lung metastasis
control	10 ± 6
0.1 mmol Capecitabine	16.6 ± 13
0.25 mmol Capecitabine	7.8 ± 7
0.5 mmol Capecitabine	3.7 ± 6
0.1 mmol 5-FCPhy	22 ± 10
0.25 mmol 5-FCPhy	6.5 ± 5
0.5 mmol 5-FCPhy	2.2 ± 5

CONCLUSIONS

The synthesis, neat and lyotropic self-assembly material behavior, in vitro toxicity, and in vivo efficacy of an amphiphile prodrug 5-FCPhy have been described. The introduction of a branched isoprenoid-type hydrocarbon chain of phytanyl (3,7,11,15-tetremethyl-hexadecyl), succeeded in promoting the formation of inverse lyotropic liquid crystalline phases, as confirmed by SAXS analysis. Inverse liquid crystalline phase formation spanned a broad temperature and concentration range, with the observed phases thermodynamically stable in excess water. The bicontinuous cubic phase initially observed under excess water conditions gradually transformed to an inverse hexagonal phase upon prolonged equilibration. The rate of transformation may be increased by increasing the equilibration temperature.

The formation of stable nanoparticles combined with its chemical stability favor the applicability of 5-FCPhy as a self-assembled slow release prodrug conjugate and a viable alternative prodrug to Capecitabine. The in vitro toxicity of 5-FCPhy displayed similar toxicity levels to Capecitabine, and significantly lower toxicity levels than 5-FU. The evaluation of 5-FCPhy for oral delivery with in vivo experiments displayed a trend of increasing efficacy with increasing dose level and improved efficacy over Capecitabine, delivered at the same dosage. Thus, 5-FCPhy self-assembled nanoparticles may be an alternative slow-release oral chemotherapeutic treatment to Capecitabine, while simultaneously capable of encapsulating other therapeutic agents, allowing for synergistic effects against a broad range of cancers.

ASSOCIATED CONTENT

Supporting Information. Synthesis of 5-FCPhy and experimental detail for TGA, DSC, XRD, cross-polarized light

microscopy, SAXS, preparation of colloidal dispersions, cryo-TEM, molecular modeling, cell culture, antiproliferative activity and in vivo experiments. This material is available free of charge via the Internet at http://pubs.acs.org/.

AUTHOR INFORMATION

Corresponding Author
*E-mail: calum.drummond@csiro.au.

ACKNOWLEDGMENT

The authors thank Prof. Gregory G. Warr from the University of Sydney for fruitful discussions, comments and provision of SAXS equipment. They are grateful to the Australian Synchrotron for awarding user time to conduct SAXS experimental work and especially thank beamline scientists, Drs. Nigel Kirby, Stephen Mudie, and Adrian Hawley for their kind assistance. The authors also acknowledge Mr Kenneth Goldie from the University of Melbourne for his help with the cryo-TEM experiments. X.G. was the recipient of a CSIRO PhD studentship. S.M. S. and C.E.C. were the recipients of CSIRO postdoctoral fellowships. C.J.D. was the recipient of an Australian Research Council Federation Fellowship.

REFERENCES

(1) Rautio, J.; Kumpulainen, H.; Heimbach, T.; Oliyai, R.; Oh, D.; Jarvinen, T.; Savolainen, J. *Nat. Rev. Drug Discovery* **2008**, *7*, 255–270.
(2) Lockett, T.; Reilly, W.; Manthey, M.; Wells, X.; Cameron, F.; Moghaddam, M.; Johnston, J.; Smith, K.; Francis, C.; Yang, Q.; Whittaker, R. *Clin. Exp. Pharmacol. Physiol.* **2000**, *27*, 563–567.
(3) Maher, S.; Leonard, T. W.; Jacobsen, J.; Brayden, D. J. *Adv. Drug Delivery Rev.* **2009**, *61*, 1427–1449.
(4) Endo, M.; Miwa, M.; Eda, H.; Ura, M.; Tanimura, H.; Ishikawa, T.; Miyazaki-Nose, T.; Hattori, K.; Shimma, N.; Yamada-Okabe, H.; Ishitsuka, H. *Int. J. Cancer* **2003**, *106*, 799–805.
(5) Hattori, K.; Kohchi, Y.; Oikawa, N.; Suda, H.; Ura, M.; Ishikawa, T.; Miwa, M.; Endoh, M.; Eda, H.; Tanimura, H.; Kawashima, A.; Horii, I.; Ishitsuka, H.; Shimma, N. *Bioorg. Med. Chem. Lett.* **2003**, *13*, 867–872.
(6) Ishitsuka, H. *Invest. New Drugs* **2000**, *18*, 343–354.
(7) Miwa, M.; Ura, M.; Nishida, M.; Sawada, N.; Ishikawa, T.; Mori, K.; Shimma, N.; Umeda, I.; Ishitsuka, H. *Eur. J. Cancer, Part A* **1998**, *34*, 1274–1281.
(8) Shimma, N.; Umeda, I.; Arasaki, M.; Murasaki, C.; Masubuchi, K.; Kohchi, Y.; Miwa, M.; Ura, M.; Sawada, N.; Tahara, H.; Kuruma, I.; Horii, I.; Ishitsuka, H. *Bioorg. Med. Chem.* **2000**, *8*, 1697–1706.
(9) Venturini, M. *Eur. J. Cancer* **2002**, *38*, 3–9.
(10) Ishikawa, T.; Utoh, M.; Sawada, N.; Nishida, M.; Fukase, Y.; Sekiguchi, F.; Ishitsuka, H. *Biochem. Pharmacol.* **1998**, *55*, 1091–1097.
(11) Ishitsuka, H.; Shimma, I.; Horii, I. *Yakugaku Zasshi—J. Pharm. Soc. Jpn.* **1999**, *119*, 881–897.
(12) Yang, L.; Alexandridis, P. *Curr. Opin. Colloid Interface Sci.* **2000**, *5*, 132–143.
(13) Drummond, C. J.; Fong, C. *Curr. Opin. Colloid Interface Sci.* **1999**, *4*, 449–456.
(14) Lynch, M. L.; Spicer, P. T. *Bicontinuous Liquid Crystals*; Taylor & Francis: Boca Raton, FL, 2005.
(15) Spicer, P. T. *Curr. Opin. Colloid Interface Sci.* **2005**, *10*, 274–279.
(16) Ulrich, A. S. *Biosci. Rep.* **2002**, *22*, 129–150.
(17) Barauskas, J.; Johnsson, M.; Tiberg, F. *Nano Lett.* **2005**, *5*, 1615–1619.
(18) Colbern, G.; Vaage, J.; Donovan, D.; Uster, P.; Working, P. *J. Liposome Res.* **2000**, *10*, 81–92.
(19) Couvreur, P.; Reddy, L. H.; Mangenot, S.; Poupaert, J. H.; Desmaele, D.; Lepetre-Mouelhi, S.; Pili, B.; Bourgaux, C.; Amenitsch, H.; Ollivon, M. *Small* **2008**, *4*, 247–253.
(20) Rose, P. G. *Oncologist* **2005**, *10*, 205–214.
(21) Mulet, X.; Kennedy, D. F.; Conn, C. E.; Hawley, A.; Drummond, C. J. *Int. J. Pharm.* **2010**, *395*, 290–297.
(22) Mezzenga, R.; Schurtenberger, P.; Burbidge, A.; Michel, M. *Nat. Mater.* **2005**, *4*, 729–740.
(23) Kogan, A.; Garti, N. *Adv. Colloid Interface Sci.* **2006**, *123*, 369–385.
(24) Yaghmur, A.; Glatter, O. *Adv. Colloid Interface Sci.* **2009**, *147—48*, 333–342.
(25) Larsson, K. *J. Dispersion Sci. Technol.* **1999**, *20*, 27–34.
(26) Fong, C.; Krodkiewska, I.; Wells, D.; Boyd, B. J.; Booth, J.; Bhargava, S.; McDowall, A.; Hartley, P. G. *Aust. J. Chem.* **2005**, *58*, 683–687.
(27) Kaasgaard, T.; Drummond, C. J. *Phys. Chem. Chem. Phys.* **2006**, *8*, 4957–75.
(28) Sagnella, S. M.; Conn, C. E.; Krodkiewska, I.; Drummond, C. J. *Soft Matter* **2009**, *5*, 4823–4834.
(29) Sagnella, S. M.; Conn, C. E.; Krodkiewska, I.; Moghaddam, M.; Seddon, J. M.; Drummond, C. J. *Langmuir* **2010**, *26*, 3084–3094.
(30) Wells, D.; Fong, C.; Krodkiewska, I.; Drummond, C. J. *J. Phys. Chem. B* **2006**, *110*, 5112–9.
(31) Conn, C. E.; Panchagnula, V.; Weerawardena, A.; Waddington, L. J.; Kennedy, D. F.; Drummond, C. J. *Langmuir* **2010**, *26*, 6240–6249.
(32) Mohammady, S. Z.; Pouzot, M.; Mezzenga, R. *Biophys. J.* **2009**, *96*, 1537–1546.
(33) Sagnella, S. M.; Gong, X.; Moghaddam, M. J.; Conn, C. E.; Kimpton, K.; Waddington, L. J.; Krodkiewska, I.; Drummond, C. J. *Nanoscale* **2011**, *3*, 919–924.
(34) Gong, X.; Moghaddam, M. J.; Sagnella, S. M.; Conn, C. E.; Danon, S.; Waddington, L. J.; Drummond, C. *J. Colloids Surf., B* **2011**, *in press*, DOI:10.1016/j.colsurfb.2011.03.007.
(35) Fong, C.; Wells, D.; Krodkiewska, I.; Hartley, P. G.; Drummond, C. J. *Chem. Mater.* **2006**, *18*, 594–597.
(36) Minamikawa, H.; Hato, M. *Langmuir* **1998**, *14*, 4503–4509.
(37) Gong, X. J.; Sagnella, S.; Drummond, C. J. *Int. J. Nanotechnol.* **2008**, *5*, 370–392.
(38) Moghaddam, M. J.; de Campo, L.; Waddington, L. J.; Drummond, C. J. *Soft Matter* **2010**, *6*, 5915–5929.
(39) Pouzot, M.; Mezzenga, R.; Leser, M.; Sagalowicz, L.; Guillot, S.; Glatter, O. *Langmuir* **2007**, *23*, 9618–9628.
(40) Chung, H.; Caffrey, M. *Biophys. J.* **1995**, *69*, 1951–1963.
(41) Conn, C. E.; Ces, O.; Mulet, X.; Finet, S.; Winter, R.; Seddon, J. M.; Templer, R. H. *Phys. Rev. Lett.* **2006**, *96*, 108102.
(42) Fong, C.; Wells, D.; Krodkiewska, I.; Weerawardeena, A.; Booth, J.; Hartley, P. G.; Drummond, C. J. *J. Phys. Chem. B* **2007**, *111*, 10713–10722.
(43) Spicer, P. T.; Hayden, K. L.; Lynch, M. L.; Ofori-Boateng, A.; Burns, J. L. *Langmuir* **2001**, *17*, 5748–5756.
(44) Caboi, F.; Borne, J.; Nylander, T.; Khan, A.; Svendsen, A.; Patkar, S. *Colloids Surf., B* **2002**, *26*, 159–171.
(45) Johnsson, M.; Barauskas, J.; Tiberg, F. *J. Am. Chem. Soc.* **2005**, *127*, 1076–1077.
(46) Sagalowicz, L.; Mezzenga, R.; Leser, M. E. *Curr. Opin. Colloid Interface Sci.* **2006**, *11*, 224–229.
(47) Sagalowicz, L.; Michel, M.; Adrian, M.; Frossard, P.; Rouvet, M.; Watzke, H. J.; Yaghmur, A.; De Campo, L.; Glatter, O.; Leser, M. E. *J. Microscopy-Oxford* **2006**, *221*, 110–121.
(48) Hyde, S. T. *Curr. Opin. Solid State Mater. Sci.* **1996**, *1*, 653–662.
(49) Rappolt, M.; Di Gregorio, G. M.; Almgren, M.; Amenitsch, H.; Pabst, G.; Laggner, P.; Mariani, P. *Europhys. Lett.* **2006**, *75*, 267–273.
(50) Nakano, M.; Sugita, A.; Matsuoka, H.; Handa, T. *Langmuir* **2001**, *17*, 3917–3922.
(51) Caboi, F.; Amico, G. S.; Pitzalis, P.; Monduzzi, M.; Nylander, T.; Larsson, K. *Chem. Phys. Lipids* **2001**, *109*, 47–62.
(52) Conn, C. E.; Darmanin, C.; Sagnella, S. M.; Mulet, X.; Greaves, T. L.; Varghese, J. N.; Drummond, C. J. *Soft Matter* **2010**, *6*, 4828–4837.
(53) Dong, Y.-D.; Tilley, A. J.; Larson, I.; Lawrence, M. J.; Amenitsch, H.; Rappolt, M.; Hanley, T.; Boyd, B. J. *Langmuir* **2010**, *26*, 9000–9010.
(54) Tomayko, M. M.; Reynolds, C. P. *Cancer Chemother. Pharmacol.* **1989**, *24*, 148–154.